CRATERING EFFICIENCY IN METAL TARGETS: RESULTS FROM IMPACT EXPERIMENTS AND 3D SCANNING. S. L. Light,[1] R. T. Daly[1], A. A. Knuth[1], and P.H. Schultz[2]. [1]The Johns Hopkins University Applied Physics Laboratory, 11101 Johns Hopkins Road, Laurel, MD, 20723, USA (siobhan.light@jhuapl.edu). [2]Department of Earth, Environmental and Planetary Sciences, Brown University, 324 Brook St., Box 1846, Providence, RI, 02912.

Introduction: Impact cratering is a key process in modifying the surfaces of all solid planets and satellites [e.g., 1]. The upcoming Psyche mission will investigate the largest M-type asteroid, 16 Psyche, which may be an exposed planetary core [2]. One of the five main objectives of this mission involves the characterization of Psyche's impact craters. Although a variety of spacecraft missions have documented what impact craters look like on rocky asteroids (e.g., NEAR, Dawn, Hayabusa, OSIRIS-REx, Hayabusa2), the Psyche mission will provide humanity's first in-depth look at impact craters on a metal-rich asteroid.

Appropriate crater scaling relationships will be required to accurately interpret craters on Psyche. Previously published experiments [3, 4] and numerical models [5] have examined the effects of oblique impact on crater morphologies in aluminum [3 – 6], lead [4], and stainless steel [4]. This contribution emphasizes how cratering efficiency (i.e., the mass of material displaced by the impact divided by the mass of the impactor) depends on variables such as the type of metal, impact velocity, impact speed, and impactor type.

Methods: During an earlier study that focused on impactor residues [7], hypervelocity impact experiments were conducted at the NASA Ames Vertical Gun Range. The experiments were done using targets of ETP copper and 6061 aluminum, multiple types of projectiles (Pyrex, quartz, agate, serpentine, basalt, and aluminum), impact angles between 15 and 90° (with respect to horizontal), and impact speeds between ~2 and 5.5 km/s (see [7] for details). Here we use these same craters in to order to further investigate cratering efficiency in metal targets as a function of these same variables.

3D scanning was used to study the morphometry of the craters (Fig. 1). Craters were scanned using the high-precision Artec Space Spider 3D scanner. The scans were edited, processed, and converted into OBJ files using proprietary Artec software. The OBJ files were then analyzed with SolidWorks, a widely used commercial software program, to determine crater volume (measured with respect to the pre-impact surface). The precision of this method was determined by taking six separate scans of each crater and processing them separately.

Shiny, reflective surfaces can degrade the quality of 3D scan products. Therefore, we assessed the accuracy of the scans by scanning copper and aluminum blocks of known dimensions. The results found at most only 1% error in volume when compared to manual measurements, a result which validates the accuracy of optical 3D scanning on these metallic surfaces. No significant difference existed between the accuracy of scans of copper and aluminum targets.

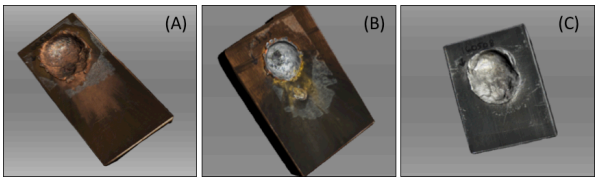

Figure 1. Meshes made from 3D scans. (A) ETP copper target; agate projectile at 2.9 km/s, 30°. (B) ETP copper target; aluminum projectile at 5.0 km/s, 30°. (C) 6061 aluminum target; quartz projectile at 5.2 km/s, 30°.

Results: Figure 3 shows the effects of target and projectile materials on cratering efficiency. These impacts were strength-dominated. We made the common assumption [e.g., 8, 9] that cratering efficiency depends only on the vertical component of the impact velocity. Nearly all experiments into copper, regardless of projectile type, fall within the 95% confidence interval for a power-law fit to the Pyrex-only data, which indicates that projectile material has minimal effects on cratering efficiency. Under these impact conditions, target material has a much greater effect: cratering efficiency is enhanced in aluminum targets compared to copper ones.

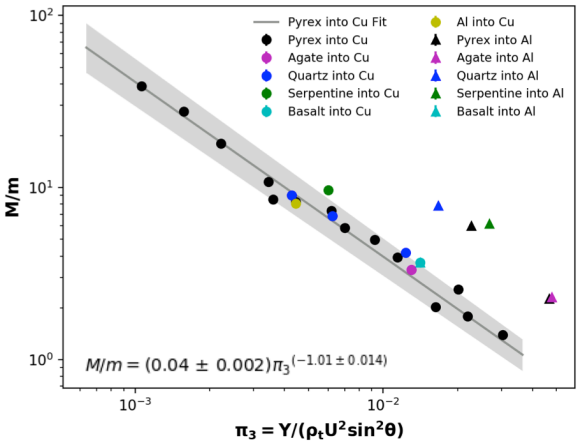

Figure 3: Results for cratering efficiency in copper and aluminum targets. The trend line and equation show the power-law fit to data from experiments with Pyrex projectiles and copper targets. Gray shading shows the 95% confidence interval for the fit. The uncertainties in the measurements are smaller than size of the data points.

Figures 4 and 5 show how impact angle affects cratering efficiency and crater planform.

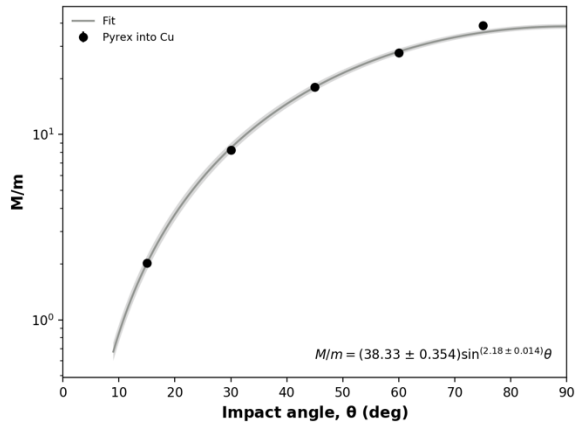

Figure 4: The relationship between impact angle, θ, and cratering efficiency, *M/m,* for Pyrex projectiles and copper targets at an impact speed of ~ 5 km/s. As θ approaches 90° (vertical), cratering efficiency increases. The data are well-fit by a $\sin^{2.2}(\theta)$ dependence, which is higher than the $\sin^2(\theta)$ dependence expected from previous experiments [e.g., 8,9] and models [5].

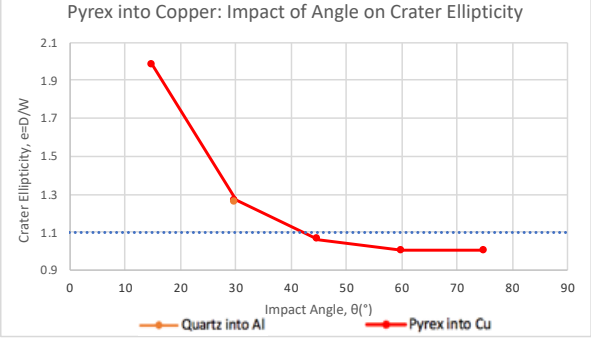

Figure 5: The relationship between impact angle and crater ellipticity, *e* (i.e., ratio between crater width parallel to, *D,* and perpendicular to, *W,* the projectile trajectory. We define craters as elliptical if *e* >1.1 [e.g. 10]. As impacts become more oblique, craters become more elliptical. The elliptical crater threshold is ~40–45° for this combination of target and projectile. Although these results are for impacts into copper, an experiment at a similar impact speed into aluminum had a comparable ellipticity at the same impact angle.

Conclusions: Copper and aluminum targets provide useful endmembers for crater scaling in metal targets. They different in density (copper is ~3.3x denser than 6061-Al), ductility (copper is far more ductile), shock impedance (copper has higher impedance), and strength (6061-Al has greater tensile and shear strengths). The impedance difference between the impactor and the target determines how much of the impact energy will be partitioned towards crater growth and excavation [11]. The larger craters observed in the aluminum targets are consistent with the material's lower impedance. The exponent derived from the power-law fit shown in Fig. 3 indicates that $\mu \approx 2/3$ which indicates that impact energy, rather than momentum, is the primary driver of overall crater volume in these experiments.

The details of 16 Psyche's surface and interior properties will not be settled until the Psyche mission arrives. However, recent estimates of 16 Psyche's bulk density are 4500±1400 kgm^{-3} [12] and 3700±500 kgm^{-3} [13]. These values are intermediate between the densities of the copper and aluminum alloy used here. However, the scaling relationship for copper targets should be more relevant to 16 Psyche because the impedance of copper is closer to the impedance of nickel-iron alloys. (The shear strengths, however, are different.) The results observed for crater ellipticity could be used to infer impact angles based on the planform of craters on Psyche. However, the cold temperatures on Psyche may lead to crater morphologies that differ from those seen here because at low temperatures iron meteorites behave in a brittle manner [14]. The observation that cratering efficiency is largely insensitive to impactor type indicates that the type of asteroid hitting Psyche (e.g., chondritic, metallic) is unlikely to affect crater volume.

Acknowledgments: The original experiments and analysis in [7] were supported by a NSF Graduate Research Fellowship (award number DGE-1058262) and NASA grant NNX13AB75G. S.L.L. conducted the work described here during the ASPIRE program at the Johns Hopkins University Applied Physics Laboratory.

References: [1] Wood, 2000, *The Solar System,* Prentice Hall. [2] Elkins-Tanton et al., 2017, *EPSC*, 11, abs. EPSC2017-384. [3] Christiansen et al., 1993, *Int. J. Impact Eng.*, 14, 157 – 168. [4] Burchell and Mackay, 1998, *J. Geophys. Res.*, 103, 22761 – 22774. [5] Davison et al., 2011, *MAPS*, 46, 1510 – 1524. [6] Schultz and Crawford, 2016, *Nature,* 535, 391 – 394. [7] Daly and Schultz, 2018, *MAPS*, 53, 1364 – 1390. [8] Chapman and McKinnon, 1986, *Satellites*, 492 – 50. [9] Gault and Wedekind, 1978, *Proc. 9th LPSC,* 374 – 376. [10] Schultz and Lutz-Garihan, 1982, *Proc. LPSC XIII,* A84–A96. [11] Gault and Heitowit, 1963, *Proc. of 6th Sixth Hypervelocity Impact Symposium*, 419 – 456. [12] Shepard et al., 2017, *Icarus*, 281, 388 – 403. [13] Hanuš et al., 2017, *A&A*, 601, A114. [14] Matsui and Schultz (1984), *JGR,* C323 – C328.